SANDIA REPORT
SAND2009-0183
Unlimited Release
Printed March 2009

Estimating IMU Heading Error from SAR Images

Armin W. Doerry

Prepared by
Sandia National Laboratories
Albuquerque, New Mexico 87185 and Livermore, California 94550

Sandia is a multiprogram laboratory operated by Sandia Corporation,
a Lockheed Martin Company, for the United States Department of Energy's
National Nuclear Security Administration under Contract DE-AC04-94AL85000.

Approved for public release; further dissemination unlimited.

Sandia National Laboratories

Issued by Sandia National Laboratories, operated for the United States Department of Energy by Sandia Corporation.

NOTICE: This report was prepared as an account of work sponsored by an agency of the United States Government. Neither the United States Government, nor any agency thereof, nor any of their employees, nor any of their contractors, subcontractors, or their employees, make any warranty, express or implied, or assume any legal liability or responsibility for the accuracy, completeness, or usefulness of any information, apparatus, product, or process disclosed, or represent that its use would not infringe privately owned rights. Reference herein to any specific commercial product, process, or service by trade name, trademark, manufacturer, or otherwise, does not necessarily constitute or imply its endorsement, recommendation, or favoring by the United States Government, any agency thereof, or any of their contractors or subcontractors. The views and opinions expressed herein do not necessarily state or reflect those of the United States Government, any agency thereof, or any of their contractors.

Printed in the United States of America. This report has been reproduced directly from the best available copy.

Available to DOE and DOE contractors from
U.S. Department of Energy
Office of Scientific and Technical Information
P.O. Box 62
Oak Ridge, TN 37831

Telephone: (865) 576-8401
Facsimile: (865) 576-5728
E-Mail: reports@adonis.osti.gov
Online ordering: http://www.osti.gov/bridge

Available to the public from
U.S. Department of Commerce
National Technical Information Service
5285 Port Royal Rd.
Springfield, VA 22161

Telephone: (800) 553-6847
Facsimile: (703) 605-6900
E-Mail: orders@ntis.fedworld.gov
Online order: http://www.ntis.gov/help/ordermethods.asp?loc=7-4-0#online

SAND2009-0183
Unlimited Release
Printed March 2009

Estimating IMU Heading Error from SAR Images

Armin Doerry
SAR Applications Department

Sandia National Laboratories
PO Box 5800
Albuquerque, NM 87185-1330

Abstract

Angular orientation errors of the real antenna for Synthetic Aperture Radar (SAR) will manifest as undesired illumination gradients in SAR images. These gradients can be measured, and the pointing error can be calculated. This can be done for single images, but done more robustly using multi-image methods. Several methods are provided in this report. The pointing error can then be fed back to the navigation Kalman filter to correct for problematic heading (yaw) error drift. This can mitigate the need for uncomfortable and undesired IMU alignment maneuvers such as S-turns.

Acknowledgements

This report was funded by the Joint DoD/DOE Munitions Program Memorandum of Understanding project. The SAR-related tasks for this project were led by George Sloan.

A special thanks goes to General Atomics Aeronautical Systems, Inc., for providing some of the data used in this report.

Thanks also to Doug Jordan, Ted Kim, and Mark Dowdican for discussions about this general topic over the past several years.

Contents

Foreword 6
1 Introduction 7
2 Executive Summary 10
3 Detailed Discussion 11
3.1 Antenna Pattern Model 11
3.2 Antenna Pointing Error Effects in the Image 14
3.3 Extracting Pointing Error from a Single Image 19
3.3.1 Method 1 – Peak Illumination Measure 20
3.3.2 Method 2 – Illumination Gradient Measure 24
3.3.3 Some Comments 26
3.4 Extracting Pointing Error from a Plurality of Images 27
3.4.1 Method 3 – Mean of Single-Image Measures 33
3.4.2 Method 4 – Overlapping Scene Content 33
3.4.3 Method 5 – Stripmap Seam Measures 34
3.4.4 Method 6 – Line-by-Line Multi-Beam Comparison 36
3.4.5 Method 7 – Sequential Lobing 38
3.4.6 Method 8 – Monopulse and Interferometry 40
3.4.7 Some Comments 41
3.5 Using Pointing Error Estimates 42
3.5.1 Mitigating Illumination Gradients 42
3.5.2 Mitigating Heading Error 43
3.6 A Note about GMTI 46
4 Conclusions 47
References 49
Distribution 50

Foreword

Precision Motion Measurement is the most difficult aspect of SAR system design and performance. There is a continuing quest for the optimum navigation instruments and system to facilitate adequate radar performance at a tolerable cost, size, and weight. There is continuing room for novelty and innovation in this arena to redefine what is optimum. This report addresses one such idea.

1 Introduction

This report concerns the proposal of aiding an Inertial Navigation Unit (IMU) or an Inertial Navigation System (INS) with information derived from a Synthetic Aperture Radar (SAR) image.

It is very typical for airborne navigation to aid alignment of an IMU with Global Positioning System (GPS) information. For straight and level flight, this works well except in one respect. While 3-dimensional accelerations can be aligned, as well as angular rotation offsets about horizontal axes (e.g. pitch and roll for a level platform), the third angular rotation axis, i.e. about the vertical axis, remains problematic. In straight and level flight, without horizontal decoupled accelerations, the orientation about the vertical axis is not observable in GPS derived measurements. A brief description of why this is true is given by Doerry.[1]

This rotational error about the vertical axis is sometimes referred to as 'yaw', and sometimes as 'heading error'. It is crucial to distinguish heading error as an error in the orientation of the IMU, and not as an error in the direction of translation of the platform. These are two separate things that are often confused.

It is important to appreciate that the geolocation capability and focusing of a SAR image (i.e. the pointing the synthetic antenna) depend on the translational motion measurement accuracy, whereas the pointing of the real antenna depends on the rotational orientation motion measurement accuracy. This fact underlies the methods and techniques described later in this report.

To first order, an excessive heading error will cause the antenna to be mis-pointed and the desired scene to be improperly illuminated by the antenna, or perhaps even not at all. The SAR image will exhibit improper reflectivity measurements, likely with a brightness gradient across the image, similar to that exhibited in Figure 1. This has a deleterious effect on Signal-to-Noise Ratio (SNR) thereby reducing image quality, and target feature detectability. In multi-phase-center antennas, any Direction of Arrival (DOA) measurements may be unacceptably impaired.

The conventional treatment for reducing heading error in a SAR system is for the platform to occasionally experience substantial lateral accelerations via dedicated maneuvers to make the heading error observable, and hence correctable. One such maneuver is the notorious S-turn. Such maneuvers are often an interruption to the platform's mission, and generally undesirable by aircraft operators and crew. Depending on the quality of the IMU and the SAR image requirements, such maneuvers might be necessary every few minutes.

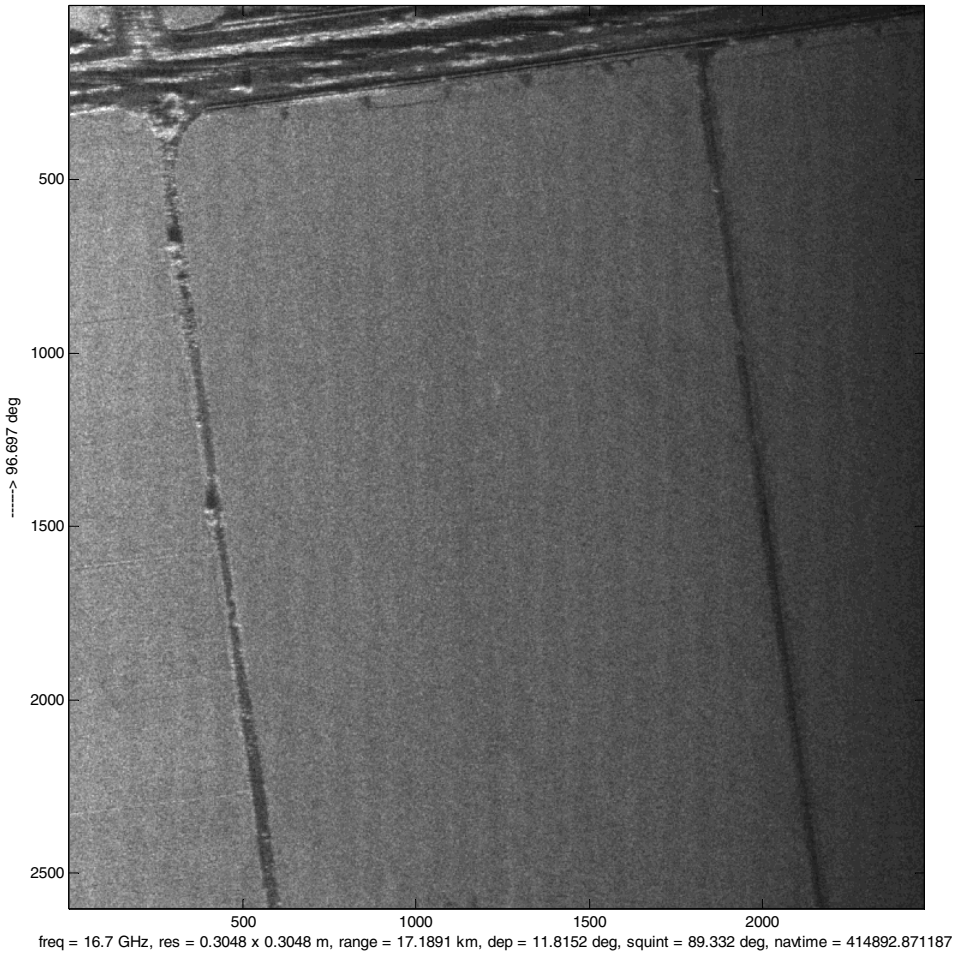

Figure 1. SAR image with enhanced brightness gradient due to simulated enhanced pointing error. (Courtesy of General Atomics Aeronautical Systems, Inc. All Rights Reserved.)

Alternatively, additional motion measurement instrumentation may be employed that makes heading errors observable, e.g. a second IMU with a transfer alignment. This is generally expensive thereby nonviable as a solution. Sometimes it is nonviable regardless of cost, due perhaps to space limitations, limited communication channels, or lack of availability of the second IMU.

One mechanism proposed earlier by Doerry[2] was to simply fix the effects of a pointing error in the image. While this works well for small pointing errors, it treats the symptom but does not address the root cause for the image degradation, namely that the IMU exhibits a heading error. Additionally, an optimal fix requires knowledge of the pointing error anyway.

Most published literature is concerned with geolocation accuracy, that is, the pointing of the synthetic antenna instead of the real antenna.

Paschall and Layne[3] discuss an integrated (GPS, INS, and SAR) targeting system that feeds SAR data back into a navigation Kalman Filter to provide improved target location accuracy. Real antenna pointing accuracy is not overtly addressed, and is not relevant to their objective.

Layne and Blasch[4] report on techniques for improving target location estimates. They use multiple SAR images to refine and improve geolocation of targets by integrating "navigation and SAR measurements in a Kalman filter." Again, real antenna pointing accuracy is not overtly addressed, and is not relevant to their objective.

Pachter and Porter[5] discuss aiding an INS using "bearings-only measurements of an unknown ground object in three-dimensional space", specifically an "optical flow measurement". They specifically address completely passive techniques to avoid "jamming, spoofing, or interference." Their technique is not suitable for, nor designed for, SAR aiding the INS.

Moreira[6] presents a method for extracting motion errors using a SAR system. However, his concern is again the translational motion of the SAR system, and does not address extracting angular rotations such as the yaw angle or heading error.

Pozgay[7] presents a method for estimating antenna pointing error using polarization ratio, but has not addressed how this might be applied to radar. This is not obvious.

We also note that radar Doppler navigation has been used effectively to aid navigation. However, these systems measure translational motion and not angular orientation. An early example is presented by Berger.[8]

Methods for correcting heading error using SAR images are not readily apparent in the published literature. Preventing the anomalies illustrated in Figure 1 seem to not have been addressed. We do so here.

2 Executive Summary

A heading error (yaw orientation error) will produce an antenna pointing error for a SAR data collection. This manifests as an apparent illumination gradient in a SAR image, and as brightness discontinuities or seams in a stripmap of SAR image patches. By measuring the gradient, and/or the discontinuity characteristics at stripmap patch seams, and/or the relationship of intensity variations as a function of antenna pointing variations, the pointing error may be calculated, and hence the heading error can be calculated. This can then be fed back to the navigation Kalman filter to improve the navigation solution, especially with respect to angular orientation.

Several methods are described below to do this. Some of them are novel.

3 Detailed Discussion

3.1 Antenna Pattern Model

The development in this report will use a relatively simple parabolic model for the antenna beam pattern. This is justified as follows.

Consider a uniformly illuminated antenna aperture. In the azimuth dimension, the normalized one-way far-field pattern will be a sinc() function, as follows

$$\Theta(\phi) = \mathrm{sinc}(b\phi) \tag{1}$$

where

$$\mathrm{sinc}(z) = \frac{\sin(\pi z)}{\pi z}$$

b = a constant that scales the input angle parameter, and
ϕ = the azimuth angular offset from the antenna beam center. (2)

The angular beam center is often called the antenna 'electrical boresight'.

The constant b is chosen such that

$$\Theta(0.5) = \mathrm{sinc}(0.5b) = \frac{1}{\sqrt{2}} . \tag{3}$$

We identify

$$b \approx 0.886 . \tag{4}$$

Furthermore, we recognize

$|\Theta(\phi)|^2 = \mathrm{sinc}^2(b\phi)$ = two-way far-field antenna field pattern,

$|\Theta(\phi)|^2 = \mathrm{sinc}^2(b\phi)$ = one-way far-field antenna normalized power gain,

$|\Theta(\phi)|^4 = \mathrm{sinc}^4(b\phi)$ = two-way far-field antenna normalized power gain. (5)

This antenna pattern has a –3 dB beamwidth of one. That is

$$\theta_{az} = 1 . \tag{6}$$

Consequently, with b defined as above, ϕ is in units of 'beamwidth'. For an arbitrary beamwidth, we need to normalize the argument with the actual beamwidth, that is, we identify

$$\Theta(\phi/\theta_{az}) = \mathrm{sinc}(b\phi/\theta_{az}) \tag{7}$$

In this case, ϕ has the same units as θ_{az}, and θ_{az} is arbitrary. That is the ratio (ϕ/θ_{az}) has units or fractional beamwidth.

We will be interested in the two-way far-field antenna field pattern. This can be expanded into the series

$$|\Theta(\phi/\theta_{az})|^2 = \mathrm{sinc}^2(b\phi/\theta_{az}) \approx 1 - \frac{(b\pi\phi/\theta_{az})^2}{3} + \frac{2(b\pi\phi/\theta_{az})^4}{45} - \frac{(b\pi\phi/\theta_{az})^6}{315} + \ldots \tag{8}$$

Note that this expansion shows a strong quadratic component, especially within the –3 dB beamwidth. If we keep just the first two terms, then we can calculate

$$|\Theta(\phi/\theta_{az})|^2 \approx 1 - \frac{(b\pi\phi/\theta_{az})^2}{3} \approx 1 - 2.58(\phi/\theta_{az})^2 . \tag{9}$$

However, this simplified approximation does not maintain precisely the original –3 dB beamwidth. Consequently, we make the modified approximation

$$|\Theta(\phi/\theta_{az})|^2 \approx 1 - 2(\phi/\theta_{az})^2 \tag{10}$$

which does maintain the original –3 dB beamwidth, and is nevertheless still accurate to within 0.4 dB inside of the –3 dB beamwidth.

If a small pointing error exists, then the pattern becomes

$$\left|\Theta\left(\frac{\phi - \phi_\varepsilon}{\theta_{az}}\right)\right|^2 \approx 1 - 2\left(\frac{\phi - \phi_\varepsilon}{\theta_{az}}\right)^2 \tag{11}$$

where

ϕ_ε = the azimuth pointing error in units of azimuth beamwidth. (12)

More generally, in two dimensions, the pattern may be described by

$$\left|\Theta\left(\frac{\phi-\phi_\varepsilon}{\theta_{az}},\frac{\varphi-\varphi_\varepsilon}{\theta_{el}}\right)\right|^2 \approx \left(1-2\left(\frac{\phi-\phi_\varepsilon}{\theta_{az}}\right)^2\right)\left(1-2\left(\frac{\varphi-\varphi_\varepsilon}{\theta_{el}}\right)^2\right), \tag{13}$$

where

φ = the elevation angular offset from the antenna beam center, and
φ_ε = the elevation pointing error, and
θ_{el} = the elevation –3 dB beamwidth. (14)

We note that it is quite typical for a SAR system to use a fan beam, where the beam shape is wider in elevation than in azimuth, often by a factor of two or more.

3.2 Antenna Pointing Error Effects in the Image

The SAR image is an array of pixels representing the measured radar reflectivity of the scene being imaged. We define the reflectivity of the scene as

$$\sigma_{\text{scene}}(x, y) \text{ = SAR scene reflectivity (linear scaling, root-power magnitude),} \tag{15}$$

where

$$\begin{aligned} x &= \text{azimuth offset distance from the scene center point, and} \\ y &= \text{slant range offset distance from the scene center point.} \end{aligned} \tag{16}$$

In general, scene reflectivity is complex, having magnitude and phase that depend on location.

We shall assume that during the course of the synthetic aperture, the radar antenna dwelled on the image scene center, that is, the radar intended to fix the electrical boresight of the antenna onto the image scene center point.

Image locations offset from the scene center location will exhibit the effects of the antenna beam illumination due to its pattern. The magnitude of the linear-scaled output pixels will be modified by the two-way far-field antenna field pattern.

Azimuth pixel offset relates to azimuth angle as

$$\tan\phi \approx x/(r_{c0} + y). \tag{17}$$

where

$$r_{c0} = \text{ nominal range to the image scene center.} \tag{18}$$

Slant range pixel offset relates to elevation angle as

$$\sin\varphi \approx \left(\frac{-y}{r_{c0} + y}\right)\tan\psi_{c0} \tag{19}$$

where

$$\psi_{c0} = \text{ nominal grazing angle to the image scene center.} \tag{20}$$

The actual antenna illumination function for the scene is then approximately modeled as

$$I_{\text{actual}}(x,y) \approx \left(1-2\left(\frac{\operatorname{atan}\left(\frac{x}{r_{c0}+y}\right)-\phi_{\varepsilon}}{\theta_{az}}\right)^2\right)\left(1-2\left(\frac{\operatorname{asin}\left(\frac{-y\tan\psi_{c0}}{r_{c0}+y}\right)-\varphi_{\varepsilon}}{\theta_{el}}\right)^2\right). \tag{21}$$

Of course, the desired illumination function is one without any angular errors, namely

$$I_{\text{ideal}}(x,y) \approx \left(1-2\left(\frac{\operatorname{atan}\left(\frac{x}{r_{c0}+y}\right)}{\theta_{az}}\right)^2\right)\left(1-2\left(\frac{\operatorname{asin}\left(\frac{-y\tan\psi_{c0}}{r_{c0}+y}\right)}{\theta_{el}}\right)^2\right). \tag{22}$$

Consequently, we identify a model for the raw scene reflectivity measurement as the scene content scaled by the illumination function, including range losses.

$$\sigma_{\text{raw}}(x,y) = \sigma_{\text{scene}}(x,y) I_{\text{actual}}(x,y)\left[\frac{r_{c0}}{r_{c0}+y}\right]^2. \tag{23}$$

Some observations are in order.

- The raw image exhibits magnitude scaling by both the antenna illumination function, as well as range losses.
- The range losses for a fixed synthetic aperture length are proportional to R^4 in power, which is equivalent to R^2 in linear scaling magnitude.
- Typical SAR systems employ a fan beam where the elevation beamwidth is greater than the azimuth beamwidth, often by a factor of two or more.
- Typical grazing angles for SAR are less than 45 degrees, and often far less.
- GPS aiding during straight and level flight is more able to help determine elevation pointing error than azimuth pointing error.

To radiometrically equalize the SAR image, the apparent illumination variations in the raw image need to be corrected. Conventionally, the image is adjusted to the form

$$\sigma_{\text{image}}(x,y) = \frac{\sigma_{\text{raw}}(x,y)}{I_{\text{ideal}}(x,y)\left[\dfrac{r_{c0}}{r_{c0}+y}\right]^2}. \tag{24}$$

This is expanded and then simplified to

$$\sigma_{\text{image}}(x,y) = \sigma_{\text{scene}}(x,y)\frac{I_{\text{actual}}(x,y)}{I_{\text{ideal}}(x,y)}. \tag{25}$$

These foregoing observations conspire to make the azimuth pointing error more readily apparent in a SAR image than the elevation pointing error, and hence more problematic. Consequently, the image model can be expanded and then reasonably simplified to

$$\sigma_{\text{image}}(x,y) = \sigma_{\text{scene}}(x,y)\left(\frac{1-2\left(\dfrac{\operatorname{atan}\left(\dfrac{x}{r_{c0}+y}\right)-\phi_{\varepsilon}}{\theta_{az}}\right)^2}{1-2\left(\dfrac{\operatorname{atan}\left(\dfrac{x}{r_{c0}+y}\right)}{\theta_{az}}\right)^2}\right). \tag{26}$$

For small SAR image range extents relative to range, this can often be reduced even further to

$$\sigma_{\text{image}}(x,y) \approx \sigma_{\text{scene}}(x,y)\left(\frac{1-2\left(\dfrac{\operatorname{atan}(x/r_{c0})-\phi_{\varepsilon}}{\theta_{az}}\right)^2}{1-2\left(\dfrac{\operatorname{atan}(x/r_{c0})}{\theta_{az}}\right)^2}\right). \tag{27}$$

For small angles measured in radians, this can be further reduced to

$$\sigma_{\text{image}}(x,y) \approx \sigma_{\text{scene}}(x,y)\left(\frac{1-2\left(\frac{(x/r_{c0})-\phi_{\varepsilon}}{\theta_{az}}\right)^2}{1-2\left(\frac{(x/r_{c0})}{\theta_{az}}\right)^2}\right). \tag{28}$$

Note that for no azimuth pointing error ($\phi_{\varepsilon}=0$), then the image correctly measures the reflectivity of the scene. However, when a pointing error exists, then the image pixel magnitudes are affected by the pointing error. So the math confirms the obvious.

What we have at this point is the following.

- The left side of the equation is a multitude of measurements. A typical SAR image might often be several million pixels, representing approximately that number of independent measurements.

- The right side of the equation contains two classes of unknowns. The first is the single number that is the azimuth pointing error, ϕ_{ε}. The second class is the multitude of target scene locations corresponding to the pixel locations in the SAR image, $\sigma_{\text{scene}}(x,y)$.

- While we can't know the 'ground truth' values for the target scene $\sigma_{\text{scene}}(x,y)$, we are often able to infer useful properties for the ground truth at least in a statistical sense. This can allow us to determine pointing error in some statistical sense.

We will capitalize on these observations for determining IMU heading error.

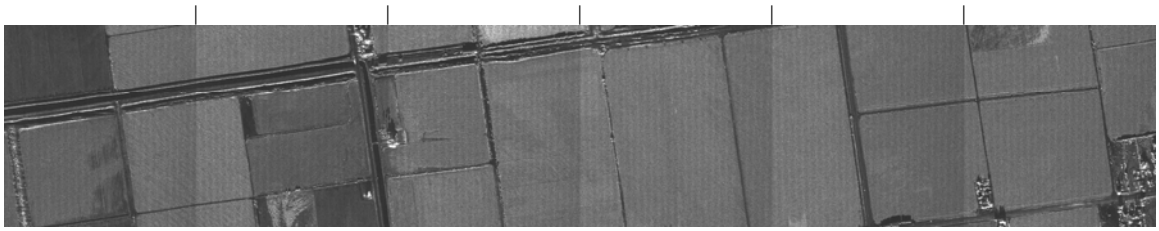

Figure 2. Segment of a stripmap SAR image exhibiting illumination seams due to antenna pointing error. Note that while some patches have fairly uniform content, others do not, even in this rural scene. This data was collected in a manner to purposely allow heading errors. (Courtesy of General Atomics Aeronautical Systems, Inc. All Rights Reserved.)

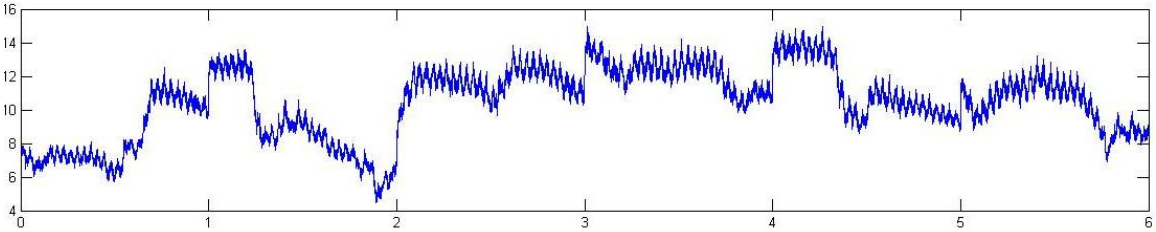

Figure 3. Representative azimuth brightness profile for the stripmap image of Figure 2. Values were calculated by taking mean of columns less 10% brightest and 10% dimmest pixel values. Note the discontinuities at image patch boundaries. Note also that within the individual patches the representative brightness varies considerably.

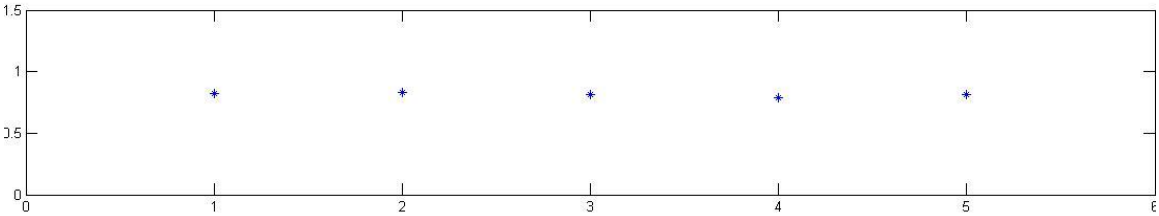

Figure 4. Ratio of pixel brightness at stripmap patch boundaries for the stripmap image of Figure 2. The ratio is of the brightness measure to the left of the scene over the brightness measure to the right of the seam. Note that the ratio is fairly stable with a mean value of about 0.812, suggesting that the pointing error itself is a relatively stable quantity, at least over the period of several stripmap patches.

3.3 Extracting Pointing Error from a Single Image

The idea here is to attempt to extract an estimate of the antenna pointing error from the properties of a single SAR image patch.

We repeat the model for the image from the previous section as

$$\sigma_{\text{image}}(x,y) \approx \sigma_{\text{scene}}(x,y)\left(\frac{1-2\left(\frac{(x/r_{c0})-\phi_{\varepsilon}}{\theta_{az}}\right)^2}{1-2\left(\frac{(x/r_{c0})}{\theta_{az}}\right)^2}\right). \tag{29}$$

The task at hand is to estimate ϕ_{ε} from $\sigma_{\text{image}}(x,y)$.

We shall presume that we have knowledge of the image geometry, including nominal range r_{c0} and the ability to extract the azimuth offset x from pixel locations. Indeed, we needed equivalent information to make the range illumination corrections. These parameters are typically available in the image header information, sometimes called 'meta-data'.

Furthermore, we shall presume that we have knowledge of the nominal azimuth beamwidth, θ_{az}.

In short, we will presume that we know everything about the model given above except explicit knowledge of $\sigma_{\text{scene}}(x,y)$ and the error we seek, ϕ_{ε}.

For convenience, we will refer to a vector from along the *x*-dimension as a 'row', and a vector from along the *y*-dimension as a 'column'.

Furthermore, we note that this technique applies essentially to the magnitude of the reflectivity functions, and consequently

$$\left|\sigma_{\text{image}}(x,y)\right| \approx \left|\sigma_{\text{scene}}(x,y)\right|\left(\frac{1-2\left(\frac{(x/r_{c0})-\phi_{\varepsilon}}{\theta_{az}}\right)^2}{1-2\left(\frac{(x/r_{c0})}{\theta_{az}}\right)^2}\right). \tag{30}$$

3.3.1 Method 1 – Peak Illumination Measure

Here we essentially remove any prior antenna pattern corrections and then find the peak of the residual illumination pattern.

We recall that $\sigma_{\text{image}}(x, y)$ has had illumination corrections applied, except that the applied azimuth correction ignored the actual pointing error. Consequently, let us consider the SAR image with the azimuth correction removed, namely

$$\sigma'_{\text{image}}(x, y) = \sigma_{\text{image}}(x, y)\left(1 - 2\left(\frac{(x/r_{c0})}{\theta_{az}}\right)^2\right). \tag{31}$$

This is now an uncorrected image, namely

$$\sigma'_{\text{image}}(x, y) = \sigma_{\text{scene}}(x, y)\left(1 - 2\left(\frac{(x/r_{c0}) - \phi_{\varepsilon}}{\theta_{az}}\right)^2\right). \tag{32}$$

This now is precisely the form that can be corrected by the technique given in reference 2. Briefly, in this technique, for each individual x-dimension pixel location, the corresponding column of pixels undergoes non-linear filtering to generate a representative pixel magnitude. The reference suggests median filtering, although others are also useful. Consequently, a single row-vector of representative pixel magnitudes is generated that represents an estimate of the azimuth illumination profile. This profile is then smoothed by fitting it to a low-order polynomial. In the referenced technique, the image is corrected by dividing each row by the smoothed estimated azimuth illumination profile.

Specifically, the technique in reference 2 calculates

$$p(x) = F_y\{\sigma'_{\text{image}}(x, y)\}, \tag{33}$$

where the desired filter is one that yields an indication of illumination, implying

$$F_y\{\sigma_{\text{scene}}(x, y)\} \approx k \tag{34}$$

where

$$k \text{ = a constant value representing typical scene reflectivity.} \tag{35}$$

This implies that

$$p(x) = F_y\{\sigma_{\text{scene}}(x,y)\}\left(1 - 2\left(\frac{(x/r_{c0}) - \phi_\varepsilon}{\theta_{az}}\right)^2\right), \tag{36}$$

The smoothing operation applied by reference 2 fits a polynomial to $p(x)$ which we identify as

$$p'(x) = \text{ polynomial fit to } p(x) \tag{37}$$

The final corrected scene is then estimated to be

$$\tilde{\sigma}_{\text{scene}}(x,y) = \sigma'_{\text{image}}(x,y)\left(\frac{k}{p'(x)}\right), \tag{38}$$

where k is estimated as the maximum value of $p'(x)$.

A byproduct of this correction is the ability to determine the row location of the peak of the smoothed estimated azimuth illumination profile $p'(x)$. We define this peak location as

$$x_{\text{illumination_peak}} = \text{value of } x \text{ at the peak of the smoothed profile.} \tag{39}$$

Once we have this value, we can estimate the heading error as

$$\phi_\varepsilon \approx \frac{x_{\text{illumination_peak}}}{r_{c0}}. \tag{40}$$

This technique hinges on the ability of the smoothed vector of filtered columns to adequately estimate the azimuth illumination profile. Some comments are in order.

- The accuracy of the estimate of the azimuth illumination profile does depend on scene content. The best scene content is featureless, with uniform statistics in all parts of the image.
- In the absence of images of featureless scenes, the column filtering attempts to generate representative values for each x position that avoids undue influence of problematic content. A median filter has shown often adequate for this task.

- Fitting the profile to a low-order polynomial further reduces the influence of anomalous column representatives. Essentially, by estimating a few polynomial coefficients from a million or more image pixels is fairly noise tolerant.

- Other things equal, the larger the image, the better the ability to estimate the pointing error. A larger image in range provides a more robust median value. A larger image in azimuth displays a more pronounced illumination profile.

Variations on this basic technique include the following.

- Instead of filtering the uncorrected image, find representative pixel values in the original erroneously corrected image, namely find

$$q(x) = F_y\{\sigma_{\text{image}}(x, y)\}. \tag{41}$$

  We can then find the illumination function

$$p(x) = q(x)\left(1 - 2\left(\frac{(x/r_{c0})}{\theta_{az}}\right)^2\right) \tag{42}$$

  and proceed as before.

- Instead of calculating $p(x)$ directly from $q(x)$, first filter $q(x)$ by fitting a line to it. That is, calculate

$$q'(x) = F_x(q(x)) = \text{linear fit to } q(x) \text{ over } x. \tag{43}$$

  Recall that for small pointing errors and uniform scene content, $q(x)$ is expected to be linear. Then we calculate

$$p(x) = q'(x)\left(1 - 2\left(\frac{(x/r_{c0})}{\theta_{az}}\right)^2\right) \tag{44}$$

  and proceed as before.

- Instead of fitting an arbitrary polynomial to $p(x)$, fit a constrained polynomial to $p(x)$, with the constraint being the form of the antenna pattern with an allowable pointing error and perhaps a scaling error.

Anecdotal evidence suggests that the correction technique of reference 2 is fairly robust for improving the aesthetic quality of a spotlight SAR image, as is illustrated in Figure 5. However, this technique is less robust for removing the seams in mosaicked patches for stripmap SAR.

Figure 5. Storage bunker complex. Image on left has no antenna pattern corrections applied. Image on right uses the correction method of reference 2. (image metadata – Ku-band, 0.1 m resolution, 3.3 km range, 31 degree grazing angle)

The stripmap in Figure 2 is comprised of six distinct image patches. From left to right, the foregoing technique allows the calculation of the following pointing errors.

1.058	degrees
–1.058	degrees
0.045	degrees
–0.158	degrees
–0.944	degrees
–0.136	degrees

These provide a mean value of –0.199 degrees, with a standard deviation of 0.767 degrees.

This suggests that the accuracy and precision of any pointing error estimate, although perhaps still useful, still leaves something to be desired.

3.3.2 Method 2 – Illumination Gradient Measure

Here we estimate the apparent beam pattern offset directly from the image illumination gradient.

Using some of the nomenclature of the previous section, the image illumination is given by

$$q(x) = F_y\{\sigma_{\text{image}}(x,y)\} \approx F_y\{\sigma_{\text{scene}}(x,y)\}\left(\frac{1-2\left(\frac{(x/r_{c0})-\phi_\varepsilon}{\theta_{az}}\right)^2}{1-2\left(\frac{(x/r_{c0})}{\theta_{az}}\right)^2}\right). \tag{45}$$

If we again assume $F_y\{\sigma_{\text{scene}}(x,y)\} \approx k$, then this reduces to

$$q(x) \approx k\left(\frac{1-2\left(\frac{(x/r_{c0})-\phi_\varepsilon}{\theta_{az}}\right)^2}{1-2\left(\frac{(x/r_{c0})}{\theta_{az}}\right)^2}\right). \tag{46}$$

For small offsets, this can be linearized over x to the approximation

$$q'(x) = F_x(q(x)) = k\left(1-2\left(\frac{\phi_\varepsilon}{\theta_{az}}\right)^2\right) + 4k\left(\frac{\phi_\varepsilon}{\theta_{az}}\right)\frac{(x/r_{c0})}{\theta_{az}}. \tag{47}$$

This may also often be adequately approximated as

$$q'(x) \approx k + 4k\left(\frac{\phi_\varepsilon}{\theta_{az}}\right)\left(\frac{(x/r_{c0})}{\theta_{az}}\right). \tag{48}$$

Consequently, once we have identified the linear fit $q'(x)$, we can estimate

$$k \approx q'(0), \tag{49}$$

and using the slope of $q'(x)$ we can then estimate

$$\phi_{\varepsilon} \approx \theta_{az}^{2}\left(\frac{r_{c0}}{4q'(0)}\right)\frac{d}{dx}\left(q'(x)\right). \tag{50}$$

With respect to the stripmap in Figure 2, from left to right, the foregoing technique allows the calculation of the following pointing errors for the respective image patches.

0.689	degrees
–1.001	degrees
0.064	degrees
–0.234	degrees
–0.540	degrees
–0.303	degrees

These provide a mean value of –0.222 degrees, with a standard deviation of 0.571 degrees.

As with the earlier method, this suggests that the accuracy and precision of any pointing error estimate, although perhaps still useful, also still leaves something to be desired.

3.3.3 Some Comments

Both of the single image techniques depend on the approximation

$$F_y\{\sigma_{\text{scene}}(x,y)\} \approx k = \text{a constant value representing typical scene reflectivity.} \quad (51)$$

As a result, the goodness of the resulting estimate for ϕ_ε depends heavily on just exactly how true this assumption really is. Accurate estimates for ϕ_ε require a high degree of fidelity for this approximation, requiring scenes with fairly uniform regional reflectivity statistics. Such scenes are normally atypical. An examination of Figure 3 shows that considerable variation often exists within any image patch, and from one image patch to the next, even the slope of the intensity measure varies and even changes sign. Consequently, single image techniques are flawed except for very controlled scene content.

One way to control image content for the purpose of estimating pointing error is to measure the 'non-idealness' of the image for this purpose and cull only those images that meet specific selection criteria. Reasonable selection criteria might include how well $q(x)$ is fit by a linear approximation $q'(x) = F_x(q(x))$. With respect to the image patches of the stripmap in Figure 2, from left to right, the respective standard deviations for the normalized difference $(q(x) - q'(x))/q'(0)$ are calculated as

0.126
0.103
0.068
0.059
0.086
0.102

This suggests that patch 4 is better than the others for estimating pointing error. A culling criteria might be to only allow pointing error estimates from images that satisfy

$$(q(x) - q'(x))/q'(0) \le \beta\,, \quad (52)$$

where

$$\beta = \text{threshold constant, for an arbitrary example 0.07.} \quad (53)$$

However, if generally controlled scene content is available, then single image techniques can be useful. This is especially true if another of our assumptions proves false, namely if the pointing error is not sufficiently stable over time.

3.4 Extracting Pointing Error from a Plurality of Images

The general idea here is to use multiple images of a scene, each with a different antenna pointing direction, to estimate the common pointing error.

All of the presumptions of Section 3.3 will still apply. In addition, we will presume that the antenna pointing error is essentially constant during the course of the collection of the multiple images required.

We again repeat the model for the image from the previous sections as

$$\sigma_{\text{image}}(x,y) \approx \sigma_{\text{scene}}(x,y)\left(\frac{1-2\left(\frac{(x/r_{c0})-\phi_{\varepsilon}}{\theta_{az}}\right)^2}{1-2\left(\frac{(x/r_{c0})}{\theta_{az}}\right)^2}\right). \tag{54}$$

We now add notation to identify among the plurality of images. Consequently, we now use the model

$$\sigma_{\text{image},n}(x,y) \approx \sigma_{\text{scene},n}(x,y)\left(\frac{1-2\left(\frac{(x/r_{c0,n})-\phi_{\varepsilon}}{\theta_{az}}\right)^2}{1-2\left(\frac{(x/r_{c0,n})}{\theta_{az}}\right)^2}\right) \tag{55}$$

where

$$n = \text{image index number.} \tag{56}$$

Furthermore, the column filtering still yields

$$q_n(x) = F_y\left\{\sigma_{\text{image},n}(x,y)\right\} \approx F_y\left\{\sigma_{\text{scene},n}(x,y)\right\}\left(\frac{1-2\left(\frac{(x/r_{c0,n})-\phi_{\varepsilon}}{\theta_{az}}\right)^2}{1-2\left(\frac{(x/r_{c0,n})}{\theta_{az}}\right)^2}\right) \tag{57}$$

However we shall no longer assume that $F_y\{\sigma_{\text{scene},n}(x,y)\}$ is adequately modeled as a constant. That is, what was previously modeled as a constant is now modeled as an image dependent function of azimuth position offset *x*, namely

$$F_y\{\sigma_{\text{scene},n}(x,y)\} = k_n(x). \tag{58}$$

This allows us to express our filtered model as

$$q_n(x) = k_n(x)\left(\frac{1-2\left(\frac{(x/r_{c0,n})-\phi_\varepsilon}{\theta_{az}}\right)^2}{1-2\left(\frac{(x/r_{c0,n})}{\theta_{az}}\right)^2}\right). \tag{59}$$

We furthermore also identify the uncorrected brightness model for each image as

$$p_n(x) = q_n(x)\left(1-2\left(\frac{(x/r_{c0,n})}{\theta_{az}}\right)^2\right) = k_n(x)\left(1-2\left(\frac{(x/r_{c0,n})-\phi_\varepsilon}{\theta_{az}}\right)^2\right). \tag{60}$$

The task at hand is as follows. Based on a measurement of $q_n(x)$, knowledge of the flight geometry, and some assumptions of $k_n(x)$, then we need to estimate ϕ_ε. The difference here from the previous section is that we have the availability of multiple images.

Prior to some detailed techniques, we provide some additional background analysis.

Consider two images, each with the antenna pointed slightly differently. We identify the first image as image n_1 and the second image as image n_2. Each image is intended to render a slightly different scene, but the scenes do overlap somewhat in azimuth. We identify within the overlapping region a pair corresponding columns, that is,

$$\sigma_{\text{scene},n_1}(x_1,y) = \sigma_{\text{scene},n_2}(x_2,y). \tag{61}$$

Consequently, representative values for these columns would also be identical, namely

$$F_y\{\sigma_{\text{scene},n_1}(x_1,y)\} = k_{n_1}(x_1) = F_y\{\sigma_{\text{scene},n_2}(x_2,y)\} = k_{n_2}(x_2). \tag{62}$$

With some foresight, we are interested in the ratio

$$\frac{p_{n_1}(x_1)}{p_{n_2}(x_2)} = \frac{k_{n_1}(x_1)\left(1-2\left(\frac{\left(x_1/r_{c0,n_1}\right)-\phi_\varepsilon}{\theta_{az}}\right)^2\right)}{k_{n_2}(x_2)\left(1-2\left(\frac{\left(x_2/r_{c0,n_2}\right)-\phi_\varepsilon}{\theta_{az}}\right)^2\right)}. \tag{63}$$

Our choice of corresponding scene columns allows the reducing this to

$$\frac{p_{n_1}(x_1)}{p_{n_2}(x_2)} = \frac{\left(1-2\left(\frac{\left(x_1/r_{c0,n_1}\right)-\phi_\varepsilon}{\theta_{az}}\right)^2\right)}{\left(1-2\left(\frac{\left(x_2/r_{c0,n_2}\right)-\phi_\varepsilon}{\theta_{az}}\right)^2\right)}. \tag{64}$$

For simplicity we identify this ratio as ρ, and note that

$$\rho_{1,2} = \frac{p_{n_1}(x_1)}{p_{n_2}(x_2)} = \left(\frac{q_{n_1}(x_1)}{q_{n_2}(x_2)}\right)\left(\frac{1-2\left(\frac{\left(x_1/r_{c0,n_1}\right)}{\theta_{az}}\right)^2}{1-2\left(\frac{\left(x_2/r_{c0,n_2}\right)}{\theta_{az}}\right)^2}\right). \tag{65}$$

Note that the right hand side of this equation is composed of entirely measured or otherwise known values. Consequently, ρ is known. This allows us to write

$$\frac{1-2\left(\frac{\left(x_1/r_{c0,n_1}\right)-\phi_\varepsilon}{\theta_{az}}\right)^2}{1-2\left(\frac{\left(x_2/r_{c0,n_2}\right)-\phi_\varepsilon}{\theta_{az}}\right)^2} = \rho_{1,2}. \tag{66}$$

The only unknown in this equation is ϕ_ε. This is the desired outcome. The task now is simply to solve this equation for ϕ_ε. This can be done in any of a variety of ways.

<u>First Solution Technique</u>

We note that the equation

$$\frac{1-2\left(z_1-z_\varepsilon\right)^2}{1-2\left(z_2-z_\varepsilon\right)^2}=\rho_{1,2} \tag{67}$$

where the various parameters are defined as

$$\begin{aligned} z_1 &= \frac{\left(x_1/r_{c0,n_1}\right)}{\theta_{az}}, \\ z_2 &= \frac{\left(x_2/r_{c0,n_2}\right)}{\theta_{az}}, \\ z_\varepsilon &= \frac{\phi_\varepsilon}{\theta_{az}}, \end{aligned} \tag{68}$$

has two real solutions for the error term z_ε, and these are

$$z_\varepsilon=\frac{-2\left(z_1-\rho_{1,2}\,z_2\right)\pm\sqrt{2}\sqrt{\left(1-\rho_{1,2}\right)^2+2\rho_{1,2}\left(z_1-z_2\right)^2}}{2\left(\rho_{1,2}-1\right)}. \tag{69}$$

Since it is expected for the pointing error to generally be small, less than the beamwidth, then we will generally choose the solution nearest zero. In fact, our concern is with

$$\left|z_1\right|,\left|z_2\right|,\left|z_\varepsilon\right|<\frac{1}{2}. \tag{70}$$

<u>Second Solution Technique</u>

Another technique might be to define an error function as

$$\gamma(z_\varepsilon) = \left(\frac{1-2(z_1 - z_\varepsilon)^2}{1-2(z_2 - z_\varepsilon)^2} - \rho_{1,2} \right). \tag{71}$$

Clearly, the correct value for z_ε is one that yields $\gamma(z_\varepsilon) = 0$. However $\gamma(z_\varepsilon)$ itself may be either positive or negative on either side of the correct value for z_ε.

The goal is then to find the value for z_ε that yields a minimum value for the error $\gamma(z_\varepsilon)$. Since two values for z_ε provide this, we will begin the search at $z_\varepsilon = 0$ and search in the direction of negative gradient, and adopting the first instance of z_ε to provide $\gamma(z_\varepsilon) = 0$, that is, the first zero crossing.

One gradient search technique is iteratively selecting values for z_ε in the following manner.

$$z_{\varepsilon,k+1} = z_{\varepsilon,k} - \frac{\gamma(z_{\varepsilon,k})}{\gamma'(z_{\varepsilon,k})} \tag{72}$$

where

$z_{\varepsilon,k}$ = the kth iteration for the estimate of z_ε, with $k \geq 0$, and
$z_{\varepsilon,0} = 0$. (73)

This is often referred to as Newton's Method. We identify

$$\gamma'(z_\varepsilon) = \frac{d}{dz_\varepsilon}\gamma(z_\varepsilon) = \frac{4(z_1 - z_\varepsilon)\left(1-2(z_2 - z_\varepsilon)^2\right) - 4(z_2 - z_\varepsilon)\left(1-2(z_1 - z_\varepsilon)^2\right)}{\left(1-2(z_2 - z_\varepsilon)^2\right)^2}. \tag{74}$$

Quite often, especially for noisy data, the convergence is overdamped by calculating

$$z_{\varepsilon,k+1} = z_{\varepsilon,k} - \mu \frac{\gamma(z_{\varepsilon,k})}{\gamma'(z_{\varepsilon,k})} \tag{75}$$

where

$$\mu \text{ = a convergence factor, typically } 0 < \mu \le 1. \tag{76}$$

For our purposes, a value closer to one, perhaps even one, is useful.

An issue is whether the derivative $\gamma'(z_{\varepsilon,k})$ is ever zero over the range of $z_{\varepsilon,k}$ likely to be encountered. This would require

$$\frac{1-2(z_2 - z_\varepsilon)^2}{(z_2 - z_\varepsilon)} = \frac{1-2(z_1 - z_\varepsilon)^2}{(z_1 - z_\varepsilon)} \tag{77}$$

in particular when

$$|z_1|, |z_2|, |z_\varepsilon| < \frac{1}{2}. \tag{78}$$

Within this range, the above conditions are only satisfied when $z_2 = z_1$, which is by design a disallowed event. Consequently, $\gamma'(z_{\varepsilon,k})$ is never zero over the range of $z_{\varepsilon,k}$ likely to be encountered.

<u>Multiple Image Estimate</u>

The previous development assumed only two images with a corresponding column. Consider now a collection of *M* images. Therewith we identify the pair-wise relationships

$$\rho_{i,j} = \frac{1-2(z_i - z_\varepsilon)^2}{1-2(z_j - z_\varepsilon)^2} \tag{79}$$

for each pair of images for all possible *i* and *j*, however such that $i \neq j$. Solving these leads to a collection of estimates for z_ε. This collection can then be averaged to find a single representative value for z_ε.

3.4.1 Method 3 – Mean of Single-Image Measures

For completeness, we mention that if we average an increasing number of multiple single-image estimates for the pointing error ϕ_ε, then their mean might be expected to converge to the true error.

For comparison to the following methods, we recall the following statistics with respect to the six image patches of Figure 2.

Method 1

mean =	–0.199	degrees
std. dev. =	0.767	degrees

Method 2

mean =	–0.222	degrees
std. dev. =	0.571	degrees

Note that the standard deviations are both a rather large fraction of the 3.2 degree antenna azimuth beamwidth.

In any case, a new recent estimate of ϕ_ε can be combined with past estimates of ϕ_ε using conventional Autoregressive Moving-Average (ARMA) processing, to provide some degree of uncertainty filtering.

3.4.2 Method 4 – Overlapping Scene Content

Here we estimate the heading error from two images with overlapping scene content, each with the antenna nominally pointed to different scene center.

For a pointing error to be measured, and ultimately corrected, it must be made obvious by suitably collecting and processing the data. Fundamentally, the real beam (due to antenna pointing) must be steered separately from synthetic beam (due to Doppler processing). Furthermore, the real beam must move between images, but the synthetic beam must remain suitably stationary. Of course a stationary synthetic beam is accomplished by corresponding z_i with z_j, requiring some degree of image overlap.

This is illustrated in Figure 6. Depending on the amount of overlap, several image columns may be processed independently, to calculate multiple estimates for z_ε. These multiple estimates may then be combined, perhaps by a calculated mean value, or other averaging techniques (e.g. median, etc.), to yield a single estimate for z_ε.

This technique is readily extended to more than two images.

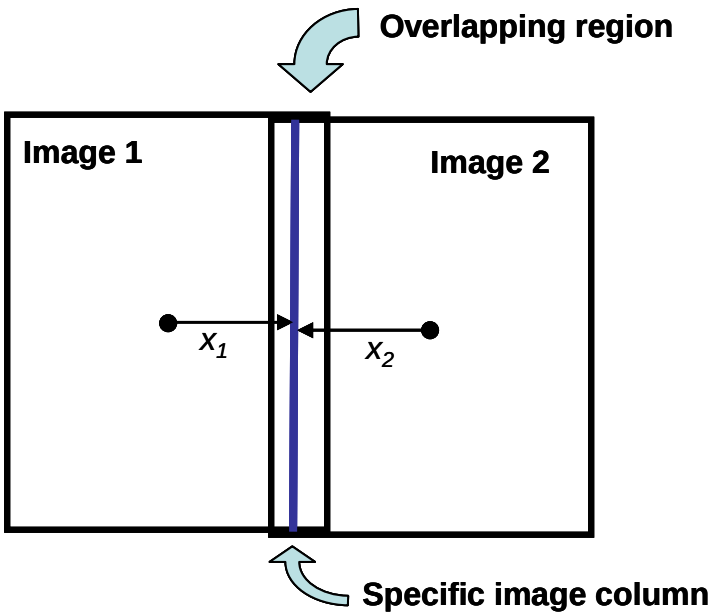

Figure 6. A corresponding column from two images is chosen, each with the antenna pointed to a different scene center.

3.4.3 <u>Method 5 – Stripmap Seam Measures</u>

Here we estimate the heading error from a stripmap image of mosaicked image patches. Let us first consider two images abutted to each other. This is illustrated in Figure 7. We may typically expect that the scene content on either side of the seam to be very similar. As a practical matter, we may expect $k_{n_1}(x_1) = k_{n_2}(x_2)$.

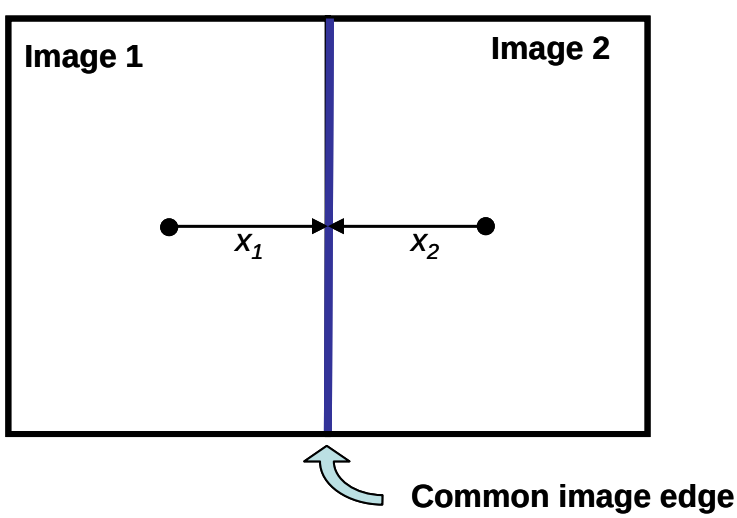

Figure 7. For two mosaicked images, we may typically expect the content on either side of the seam to be for all intents and purposes identical.

For a sequence of M images, there will be $(M-1)$ seams to exploit. This leads to $(M-1)$ individual estimates of pointing error, which may be averaged in some fashion (e.g. mean, median, etc.). The algorithm is illustrated in Figure 8.

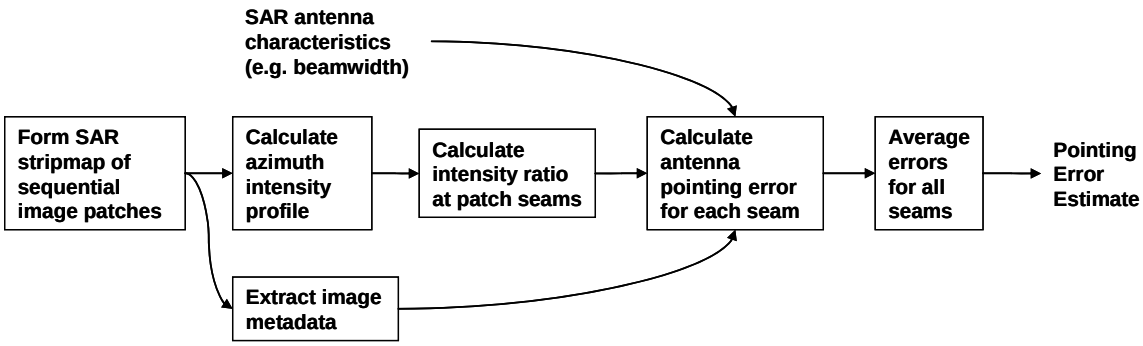

Figure 8. Block diagram of processing steps for Method 5 – Stripmap Seam Measures.

Furthermore, for a stripmap of M images, the images often have similar geometries and identical widths, that is, for each pair $z_2 = -z_1$. Furthermore yet, this allows us to calculate directly

$$\rho_{1,2} = \left(\frac{q_{n_1}(x_1)}{q_{n_2}(x_2)} \right). \tag{80}$$

For a relatively small set of images, we can expect the pointing error to be relatively stable. This is precisely the observation in Figure 4. This allows us to average the brightness ratios across the seams directly, and then perform the pointing error calculations only once on the averaged ratio $\rho_{1,2}$.

The stripmap in Figure 2 yields five seams from which we calculate a mean pointing error of –0.194 degrees, with a standard deviation of 0.018 degrees. This indicates a greater degree of confidence in this method over that of averaging single-image techniques.

3.4.4 Method 6 – Line-by-Line Multi-Beam Comparison

Heretofore, we have presumed that the basic data collection mode is one of spotlight SAR, where a single synthetic aperture is associated with a single image, and the antenna is pointed at a single constant scene center for that particular synthetic aperture's image. Even stripmap generation has been presumed to be the result of mosaicked spotlight image patches.

We now briefly discuss an alternate data collection mode where the center of the antenna beam footprint is also scanned at a rate commensurate with the radar platform velocity. Consequently, each radar pulse is aimed at a different point on the ground.[†] Some SAR systems prefer this collection mode for generating stripmap images. These are often formed in a manner such that no image patch seams are obvious in the stripmap, even when pointing errors are present. Sometimes this is called "line-by-line" processing, and sometimes "conventional" stripmap processing. A pointing error would manifest typically as a reduction in the radar reflectivity measured in the desired synthetic beam.

However, even with line-by-line processing, any synthetic aperture can be resolved into multiple synthetic antenna beams. This is, after all, precisely what is done with patch processing. As the desired synthetic beam is employed to form a stripmap image, so too can adjacent or offset synthetic beams be employed to form duplicate stripmaps, but either delayed or advanced in time, and from different parts of the real antenna beam. This is illustrated in Figure 9 and Figure 10. If the real antenna beam has a pointing error, then some offset synthetic beam will generate a stripmap with a greater intensity than the desired synthetic beam. The offset angle of the brightest (highest average intensity) synthetic beam is precisely the antenna pointing error.

With a sufficient number of synthetic beam directions monitored (at least three, but more is better) then a model of the antenna beam pattern can be fit to the relative average intensity measurements, and a peak direction therewith determined.

[†] Sandia SAR systems have traditionally designated this as "Mode 4". The technique of dwelling on a scene center with the antenna beam has traditionally been designated as "Mode 5".

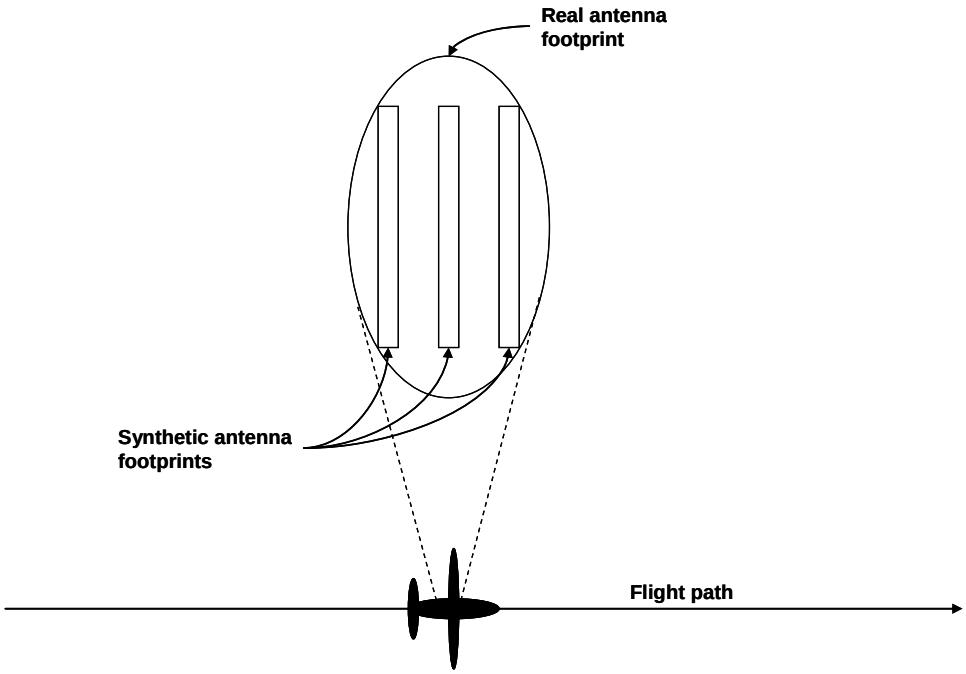

Figure 9. Resolving real antenna footprint into multiple synthetic antenna footprints.

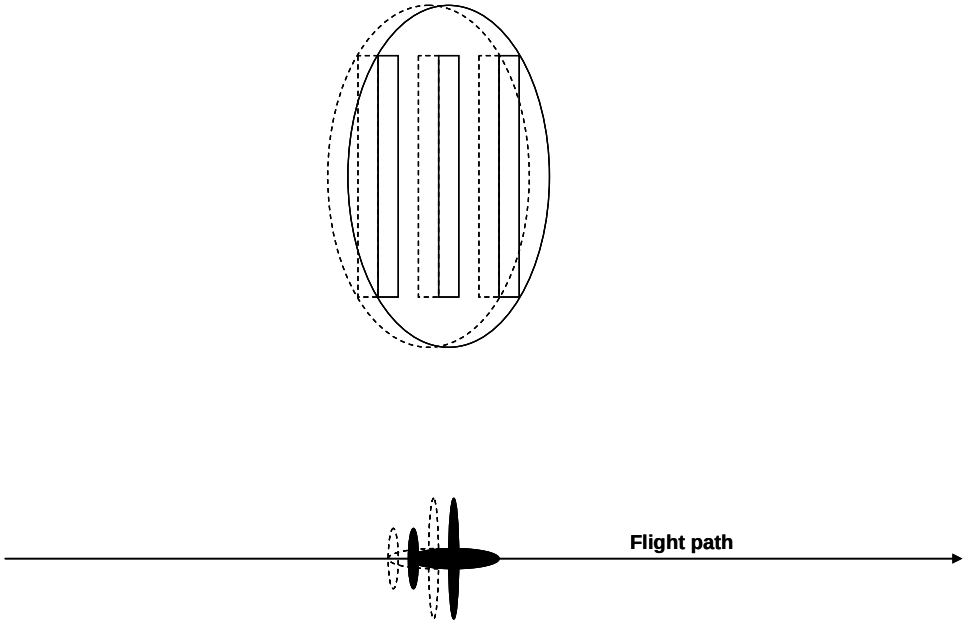

Figure 10. As the radar translates, so do the synthetic beams, covering the same ground over the course of a long data collection.

3.4.5 Method 7 – Sequential Lobing

Here we borrow an idea from the early days of tracking radars, namely sequential lobing for direction finding[9], except that we adapt it to finding antenna pointing error. Our adaptation is to purposely offset the antenna beam center from the direction of the SAR image center, and do so differently for at least two images of the same scene. This is illustrated in Figure 11.

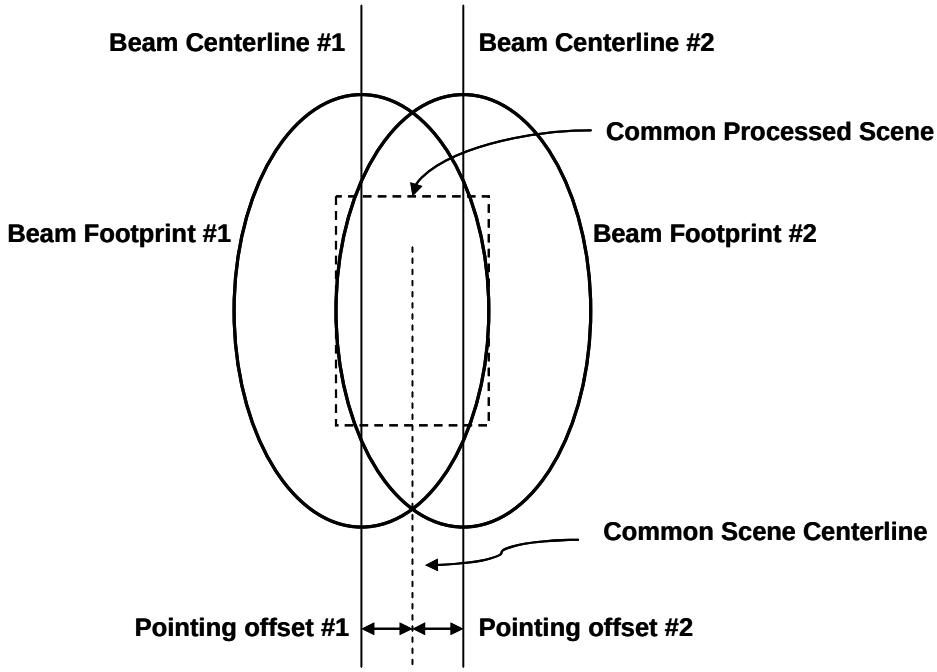

Figure 11. Sequential Lobing offsets the antenna beam boresight from the desired scene center by different amounts in two or more images.

We define the antenna pointing offset as

$$\phi_{p,n} = \text{antenna pointing offset for the } n^{\text{th}} \text{ image.} \tag{81}$$

Then the image can be expressed as

$$\sigma_{\text{image},n}(x,y) \approx \sigma_{\text{scene},n}(x,y)\left(\frac{1-2\left(\frac{\left(x/r_{c0,n}\right)-\phi_{p,n}-\phi_{\varepsilon}}{\theta_{az}}\right)^2}{1-2\left(\frac{\left(x/r_{c0,n}\right)-\phi_{p,n}}{\theta_{az}}\right)^2}\right). \tag{82}$$

Using the simplified notation previously developed, we still identify

$$\frac{1-2\left(z_1-z_\varepsilon\right)^2}{1-2\left(z_2-z_\varepsilon\right)^2}=\rho_{1,2} \tag{83}$$

but now where

$$z_1=\frac{\left(x_1/r_{c0,n_1}\right)-\phi_{p,n_1}}{\theta_{az}},$$
$$z_2=\frac{\left(x_2/r_{c0,n_2}\right)-\phi_{p,n_2}}{\theta_{az}},$$
$$z_\varepsilon=\frac{\phi_\varepsilon}{\theta_{az}}, \tag{84}$$

and

$$\rho_{1,2}=\left(\frac{q_{n_1}\left(x_1\right)}{q_{n_2}\left(x_2\right)}\right)\left(\frac{1-2\left(\frac{\left(x_1/r_{c0,n_1}\right)-\phi_{p,n_1}}{\theta_{az}}\right)^2}{1-2\left(\frac{\left(x_2/r_{c0,n_2}\right)-\phi_{p,n_2}}{\theta_{az}}\right)^2}\right). \tag{85}$$

If both images are of the exact same scene, and we ensure that the images are suitably registered, then

$$x_1=x_2\text{, for any and all locations } x_i. \tag{86}$$

and we may simplify

$$\rho_{1,2}=\left(\frac{q_{n_1}\left(x_i\right)}{q_{n_2}\left(x_i\right)}\right)\left(\frac{1-2\left(\frac{\left(x_i/r_{c0,n_1}\right)-\phi_{p,n_1}}{\theta_{az}}\right)^2}{1-2\left(\frac{\left(x_i/r_{c0,n_2}\right)-\phi_{p,n_2}}{\theta_{az}}\right)^2}\right),$$

$$z_1=\frac{\left(x_i/r_{c0,n_1}\right)-\phi_{p,n_1}}{\theta_{az}},$$
$$z_2=\frac{\left(x_i/r_{c0,n_2}\right)-\phi_{p,n_2}}{\theta_{az}}, \tag{87}$$

for all possible x_i locations in the images.

With this method, and these definitions, we can find an estimate of ϕ_ε for any choice of x_i using any of the techniques discussed earlier. If we find an estimate of ϕ_ε for every possible x_i, then we can merely average them for a single answer.

The procedure is illustrated in Figure 12.

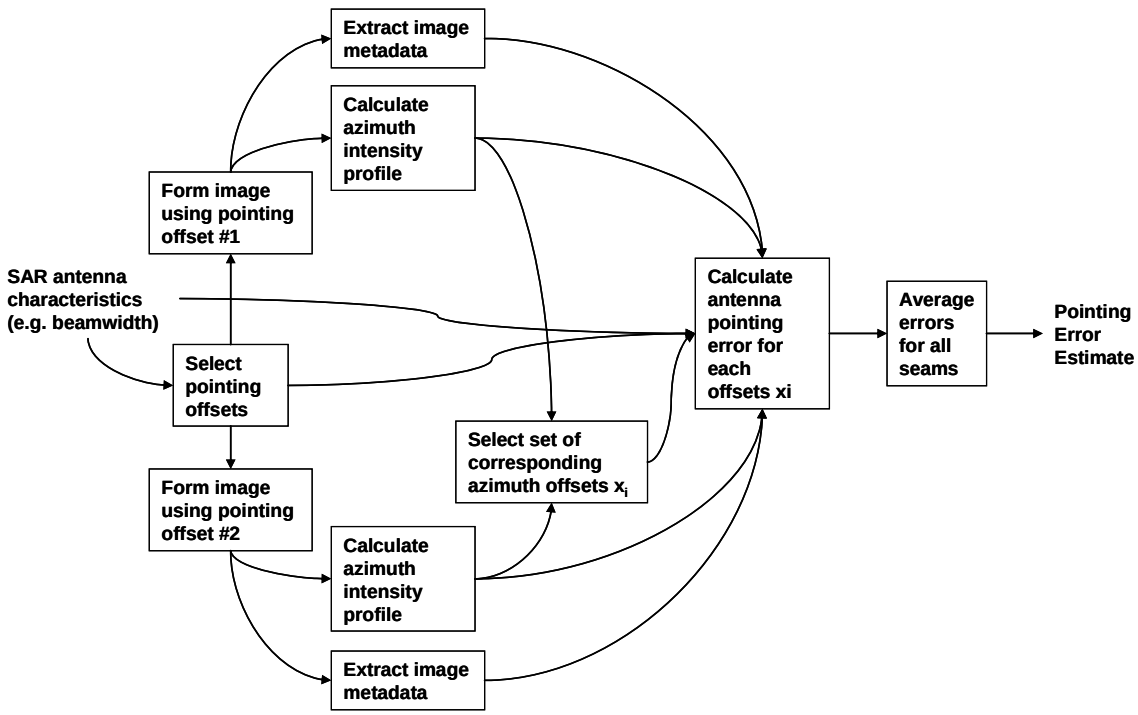

Figure 12. Procedure for implementing Method 7 – Sequential Lobing for calculating antenna pointing error.

3.4.6 <u>Method 8 – Monopulse and Interferometry</u>

Multiple antenna phase centers, or equivalent, can substantially aid the measurement of pointing error.

With respect to the previous section (Method 7 – Sequential Lobing), if both lobes could be generated at the same time, and their data distinguished from each other, then data from the same set of radar pulses could be used to determine the pointing error. This is precisely the function of Monopulse antennas.[10] Equivalent images generated from left and right lobes could be processed as in the previous section.

More generally, a difference between multiple phase centers or amplitude lobes can be generated that provides a null in the direction of the electrical boresight of the combined antenna. This null is fairly sharp, and its direction is desired to be towards the scene center of the processed SAR images. The angular difference between the null direction and the scene center direction is the pointing error of the antenna.

This of course assumes we are dealing with stationary clutter rather than moving vehicles as targets.

3.4.7 Some Comments

The principal problem with single-image techniques has been the presumption that regional reflectivity statistics were essentially constant over the entire image, that is, $F_y\{\sigma_{\text{scene}}(x, y)\} \approx k$. Multiple-image techniques eliminate (or substantially relax) this constraint.

Even in the case of Method 5, we would expect the statistics on either side of a stripmap seam to be much more similar than the statistics on opposite sides of the image patch, as are essentially compared in Methods 1 and 2. In our measurements of Figure 2 this manifests as a substantially reduced standard deviation for the pointing error estimate.

While we expect that the multiple-image techniques will yield a better estimate of pointing error than single-image techniques, these do in fact rely on the pointing error to be essentially stable and constant over the course of collection of the multiple images.

We also note that variations on the techniques described herein are innumerable.

Of the methods described, Method 5 – Stripmap Seam Measures is probably the easiest to retrofit into existing SAR systems as it makes use of a fairly typical and ordinary stripmap imaging mode. It can also be used during the course of normal stripmap imaging. The most effective is expected to be Method 7 – Sequential Lobing, as it provides the largest amount of corresponding scene content for the fewest number of images. This makes Method 7 – Sequential Lobing the preferred technique for accuracy, although it necessitates the implementation of a new dedicated imaging mode. Of course, if a multi-phase-center antenna is employed, then Method 8 – Monopulse and Interferometry becomes the preferred technique.

3.5 Using Pointing Error Estimates

The purpose of estimating antenna pointing error is two-fold.

1. to correct the image illumination gradients for current images, and

2. to feed back to the navigator for improved heading error estimates, thereby minimizing image illumination gradients for future images.

We note that for either purpose, image azimuth resolution is not as important as having a large fraction of the azimuth antenna beam footprint in the image, so that the anomalous gradients are obvious. Coarse resolutions are quite adequate.

3.5.1 <u>Mitigating Illumination Gradients</u>

A byproduct of accurate pointing error estimates is the ability to correct the anomalous illumination gradients in SAR images, most notable in stripmap images as seams between the adjacent image patches.

We now illustrate this by using the results of Method 5 to correct the illumination of the individual image patches in the stripmap of Figure 2.

By combining several previous results, we estimate the final corrected scene to be

$$\tilde{\sigma}_{\text{scene}}(x,y) = \sigma_{\text{image}}(x,y)\left(\frac{1-2\left(\frac{(x/r_{c0})}{\theta_{az}}\right)^2}{1-2\left(\frac{(x/r_{c0})-\phi_{\varepsilon}}{\theta_{az}}\right)^2}\right). \tag{88}$$

We illustrate the results of this in Figure 13 where we repeat the stripmap segment of Figure 2 on the top, and the corrected version on the bottom. Note the mitigation of the seams between the adjacent image patches.

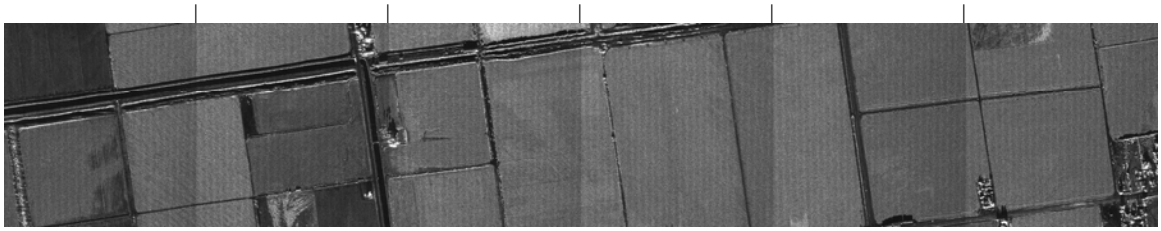

(a)

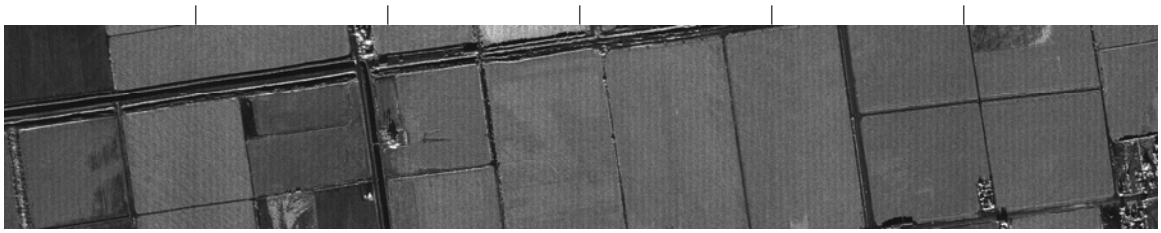

(b)

Figure 13. (a) Original stripmap from Figure 2, and (b) corrected stripmap using pointing error estimate using Method 5. Hash marks indicate seams. (Courtesy of General Atomics Aeronautical Systems, Inc. All Rights Reserved.)

3.5.2 Mitigating Heading Error

Heading error is the yaw angle orientation error about a locally vertical axis. Antenna azimuth pointing error is an angular orientation error about an axis that is normal to the line-of-sight direction to the desired boresight and contained in a locally vertical plane. This is illustrated in Figure 14.

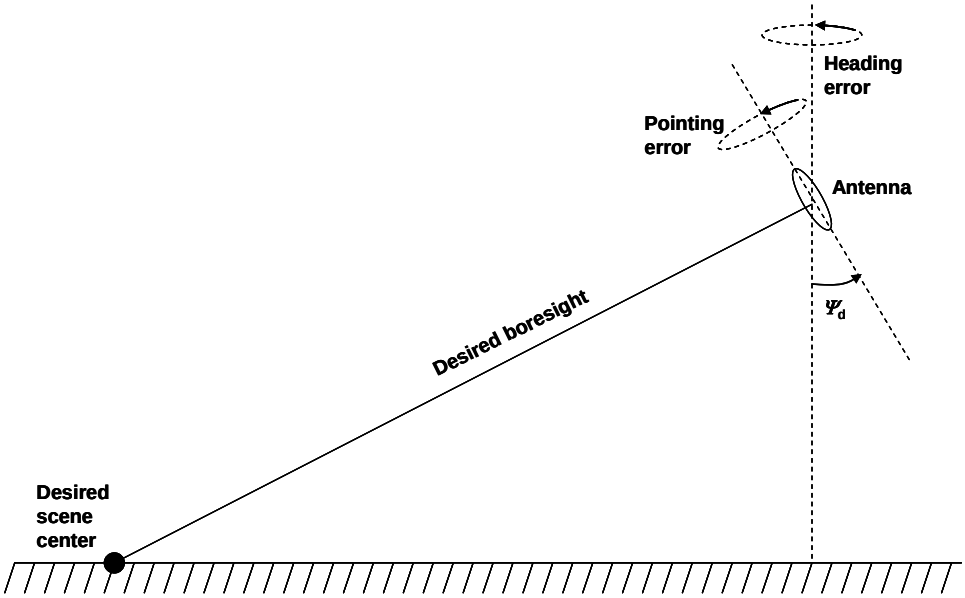

Figure 14. Geometry relating antenna azimuth pointing error to heading error.

We will assume that any refraction or other atmospheric effects are negligible. For small pointing errors, we calculate the heading error as

$$\theta_\varepsilon = \phi_\varepsilon \sec\psi_d \tag{89}$$

where

$$\psi_d = \text{local depression angle of the desired antenna boresight.} \tag{90}$$

Generally, the heading error will be somewhat greater than the pointing error. The factor is the secant of the depression angle.

A typical procedure for aligning a GPS-aided IMU with respect to heading error is to excite lateral accelerations via intentional maneuvers such as S-turns, whenever it is expected that the IMU has sufficient uncertainty in this regard. Depending on the quality of the IMU (actually its rate gyros), the period of problematic uncertainty growth may be from low-digit minutes to many hours.

S-turns are problematic because they are uncomfortable for crew and passengers of manned aircraft, and may interrupt mission activities for any aircraft. Depending on the platform, S-turns or equivalent maneuvers may not even be possible. Therefore, it is desirable to align the heading of an IMU without S-turns or equivalent. This necessitates measuring actual heading error in some other fashion. Measuring antenna pointing error with adequate accuracy and precision does just this.

IMU heading alignment requires feeding back the calculated antenna pointing error (transmogrified to heading error) to the navigation Kalman filter. This can happen on one or both of the following schedules.

1. During the course of normal SAR operation, as opportunity allows.

   This might include single-image techniques during spotlight SAR operation (Methods 1 and 2), and stripmap seam measures during stripmap SAR operation (Method 5).

2. At scheduled intervals that depend on the expected error growth rate.

   This might include short short stripmap operations with associated stripmap seam measures (Method 5), or dedicated sequential lobing alignment operations (Method 7).

Monopulse and.or interferometric techniques can be used on either schedules. The details of incorporating any of these measures into the navigation Kalman filter are beyond the scope of this report.

The general procedure for feeding pointing error information back to the navigation Kalman filter is illustrated in Figure 15.

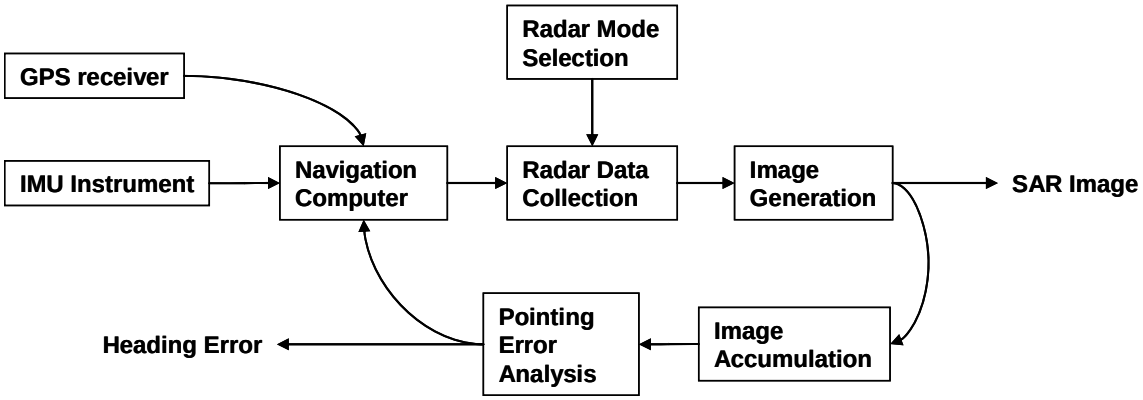

Figure 15. General procedure for pointing error feedback to navigation computer.

3.6 A Note about GMTI

The foregoing discussion has centered around SAR. However, any Doppler processing will facilitate the methods described. This includes exo-clutter GMTI.

Note that an intermediate step in GMTI processing is to form a range-Doppler map of the echoes received. Although Doppler is associated in GMTI with target vehicle velocity, the range-Doppler map also generally clearly exhibits a Doppler band of clutter returns. Furthermore, the position in Doppler where the clutter band appears is quite predictable. The degree to which the clutter band is offset from its predicted location is in fact proportional (by a known factor) to the antenna azimuth pointing error. The clutter band is essentially a coarse-azimuth resolution SAR image, and without any antenna azimuth pattern corrections applied.

While single-image techniques for estimating pointing error might be adequately adapted, GMTI modes that ratchet dwell spots typically overlap their beam positions from one dwell to the next. This makes variations of Method 4 – Overlapping Scene Content a particularly viable technique for opportunistic pointing error measurements and calculations.

The bottom line is that not juat SAR modes are useful for pointing error estimation. GMTI modes can be adapted as well.

4 Conclusions

The following points are worth repeating.

- IMU translational errors affect the synthetic antenna pointing, and hence geolocation errors. IMU angular orientation errors affect the real antenna pointing, and hence the illumination of the desired scene. These are somewhat independent of each other.

- Heading errors are proportional to real antenna pointing errors.

- Antenna pointing errors manifest as illumination gradients in a SAR image.

- Measures of the illumination gradient can be used to estimate antenna pointing error, and hence heading error.

- Individual images can be used to estimate pointing error, but provide very noisy estimates, subject to scene content.

- Using multiple images can overcome the scene content problems of the single-image techniques, providing considerably less noisy estimates of pointing error. Multiple-image techniques are feasible because pointing errors are expected to be fairly stable over the course of several images.

The novelty disclosed in this report includes principally the following

- Two or more SAR images that contain related scene content but have different antenna pointing directions may be used to robustly estimate antenna pointing error, even for single-phase-center SAR systems.

- The most effective methods for this are

  Method 5 – Stripmap Seam Measures
  Method 7 – Sequential Lobing

"Failure is only the opportunity to begin again more intelligently."
-- Henry Ford

References

[1] Armin W. Doerry, "Motion Measurement for the Lynx SAR", Sandia Report SAND2009-0437, Official Use Only – General Atomics Proprietary Information, March 2009.

[2] Armin W. Doerry, "Automatic Compensation of Antenna Beam Roll-off in SAR Images", Sandia Report SAND2006-2632, Unlimited Release, April 2006.

[3] Major Randall N. Paschall, J. R. Layne, "Design and Analysis of an Integrated Targeting System", *Proceedings of the IEEE 1994 National Aerospace and Electronics Conference*, NAECON 1994, vol.2, pp. 937-944, Dayton, OH, USA, 23-27 May 1994.

[4] Jeffery R. Layne, Lt. Erik P. Blasch, *Integrated Synthetic Aperture Radar and Navigation Systems for Targeting Applications*, Wright Laboratory Report WL-TR-97-1185, September 1997.

[5] Meir Pachter, Alec Porter, "Bearings-Only Measurements for INS Aiding: The Three-Dimensional Case", *Proceedings of the 2004 American Control Conference*, Vol. 6, pp. 5363-5368, Boston, Massachusetts, USA, 30 June - 2 July 2004.

[6] Joao Moreira, "Method for extracting motion errors of a platform carrying a coherent imaging radar system from the raw radar data and device for executing the method", US Patent 5,166,688, November 24, 1992.

[7] Jerome H. Pozgay, "Estimating an antenna pointing error by determining polarization", US Patent 6,961,016, November 1, 2005.

[8] France B. Berger, "Aircraft Drift Angle Measuring Instrument", US Patent 2,857,590, October 21, 1958.

[9] M. Skolnik, *Radar Handbook*, second edition, ISBN 0-07-057913-X, McGraw-Hill, Inc., 1990.

[10] Samuel M. Sherman, *Monopulse Principles and Techniques*, ISBN 0-89006-137-8, Artech House, Inc., 1984.

Distribution

Unlimited Release

1	MS 1330	B. L. Burns	5340
1	MS 0519	T. J. Mirabal	5341
1	MS 1330	M. S. Murray	5342
1	MS 1330	W. H. Hensley	5342
1	MS 1330	S. D. Bensonhaver	5342
1	MS 1330	T. P. Bielek	5342
1	MS 1330	J. D. Bradley	5342
1	MS 1330	A. W. Doerry	5342
1	MS 1330	D. W. Harmony	5342
1	MS 1330	J. A. Hollowell	5342
1	MS 1330	C. Musgrove	5342
1	MS 1330	S. Nance	5342
1	MS 1330	R. Riley	5342
1	MS 1330	J. A. Rohwer	5342
1	MS 1330	B. G. Rush	5342
1	MS 1330	G. J. Sander	5342
1	MS 1330	D. G. Thompson	5342
1	MS 0501	P. R. Klarer	5343
1	MS 1330	K. W. Sorensen	5345
1	MS 0529	B. C. Brock	5345
1	MS 1330	D. F. Dubbert	5345
1	MS 0529	G. K. Froehlich	5345
1	MS 1330	F. E. Heard	5345
1	MS 1330	G. R. Sloan	5345
1	MS 1330	S. M. Becker	5348
1	MS 1330	O. M. Jeromin	5348
1	MS 1330	S. A. Hutchinson	5349
1	MS 0519	D. L. Bickel	5354
1	MS 0501	M. Dowdican	5338
1	MS 0501	J. D. Jordan	5338
1	MS 0501	T. J. Kim	5338
1	MS 0899	Technical Library	9536 (electronic copy)

;-)